

Aggregating Long-Term Context for Learning Surgical Workflows

Yutong Ban^{1,2}, Guy Rosman^{2,3}, Thomas Ward¹, Daniel Hashimoto¹
Taisei Kondo⁴, Hidekazu Iwaki⁴, Ozanan Meireles¹, and Daniela Rus²

¹ SAIL, Massachusetts General Hospital, 55 Fruit Street, Boston, MA, US

² Distributed Robotics Laboratory, CSAIL, MIT, 32 Vassar St, Cambridge, MA, US

³ Toyota Research Institute, Cambridge, MA, US

⁴ Olympus Corporation, Tokyo, Japan

Abstract. Analyzing surgical workflow is crucial for computers to understand surgeries. Deep learning techniques have recently been widely applied to recognize surgical workflows. Many of the existing temporal neural network models are limited in their capability to handle long-term dependencies in the data, instead relying upon strong performance of the underlying per-frame visual models. We propose a new temporal network structure that leverages task-specific network representation to collect long-term sufficient statistics that are propagated by a sufficient statistics model (SSM). We leverage our approach within an LSTM backbone for the task of surgical phase recognition and explore several choices for propagated statistics. We demonstrate superior results over existing state-of-the art segmentation and novel segmentation techniques, on two laparoscopic cholecystectomy datasets: the already published Cholec80 dataset and MGH100, a novel dataset with more challenging, yet clinically meaningful, segment labels.

Keywords: surgical video · work flow recognition · temporal context aggregation.

1 Introduction

The future of computer-assisted laparoscopic surgery relies upon a strong fundamental automated understanding of surgical workflow from videos. While significant work has been performed in improving the understanding of video [17,20,5,10,22] and producing better annotation and supervision cues [17,8,16], existing models still fall short of a complete and automatic interpretation of surgery. Unlike the progress made in interpreting images from reconstructive modalities such as Computed Tomography (CT) or Magnetic Resonance Imaging (MRI) [12], surgery is a temporal process with only weakly observable visual-cues which requires reasoning over the whole temporal process.

Current computer vision efforts in surgical workflow analysis have addressed operative phase recognition and prediction of remaining surgery duration. Initial

works used combined model architectures of Support Vector Machines (SVM) with Hidden Markov Models (HMM) [20] or Convolutional Neural Networks (CNN) with SVM and Hierarchical HMM [17]. The majority of approaches now use a CNN with a Long-Short Term Memory (LSTM) backbone [6,1,18], sometimes with modifications such as Prior Knowledge Inference (PKI) (hand-crafted knowledge of operative phase workflow to limit incorrect inferences of already finished phases) [7] or "multitask" architectures that incorporate multiple streams of inference in addition to operative phase labels to improve identification (e.g. tool prediction [8] or kinematics and robotic system events [16]).

In many of the methods above, the underlying temporal model is limited in its capability to analyze temporal information across time scales. HMMs are inherently Markovian; and LSTMs are limited by their ability to propagate gradients in time [3,15,19]. Models such as dilated temporal convolutions and hidden semi-Markov models (HSMMs) are limited in their ability to efficiently train information flow across long periods of time, with the latter limited by its inference computational efficiency.

Understanding surgical workflows requires reasoning about events across highly varied temporal scales, from a few seconds to hours, exceeding the capabilities of existing models. For example, in laparoscopic cholecystectomy, "Dissection of Calot's triangle" involves removing the lower portion of the gallbladder from the liver bed (i.e. clearing the cystic plate). This phase can be visually indistinct from "Removal of the Gallbladder from the Liver Bed" later in the case and requires knowledge that key phases (occurring minutes later) have not yet occurred to accurately infer the current surgical phase. In such cases, information extracted by LSTM remains local compared to the total duration of the surgery and fails to improve classification performance. The effective use of long-term temporal information remains an open question. We try to address the problem by aggregating the long-term temporal context through several sufficient statistic models (SSM) and combine them with visual cues to feed into an LSTM. The SSM models then use the updated LSTM results to refine the global context features.

Our paper's contributions can be summarized as (i) a novel SSM-LSTM framework that aggregates the long-term temporal context of different time scales to assist with LSTM inference; (ii) validation of the proposed model on two large laparoscopic video datasets – the previously-published Cholec80, and LC100, a novel dataset – with state-of-the-art performance on both datasets.

2 Methods

We introduce an architecture to better leverage long-term temporal information in surgical phase recognition via approximate sufficient statistic features. We then proceed to detail a set of approximate sufficient statistic features included within the proposed architecture.

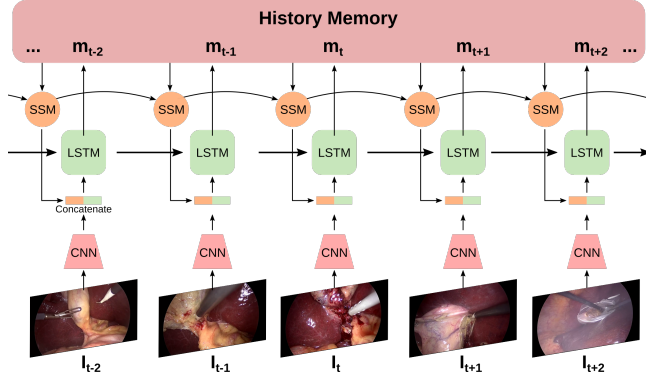


Fig. 1. SSM network architecture. Information from the network phase estimation head is processed as a multichannel temporal signal. The resulting statistics are concatenated with the visual embeddings and passed to the LSTM.

2.1 Model Architecture

Surgical phase recognition attempts to classify the correct surgical phase label given video frames $\mathbf{I}_t, t = 0 \dots T$. We denote the ground truth label for frame \mathbf{I}_t by $y_t \in 1 \dots N$, where N is the number of different surgical phases. We process individual frames via a CNN visual model (based on ResNet), encoding the visual content as a single vector \mathbf{v}_t , which is then fed to the LSTM, forming a standard CNN+LSTM structure.

In analyses of temporal processes, recurrent neural networks such as LSTMs perform well when inference relies mainly on recent information. However, performance suffers when long-term temporal information is required for inference. To address the lack of long-term information, dilated convolutions [21] have been suggested, but they fail to leverage several phenomena involved in the interpretation of surgeries:

1. Correct classification of phase transitions depends on propagation of low-dimensional information that coincides with the actual phases being detected.
2. Short events that are from the distant past can significantly affect interpretation of the current observations. (e.g. clearing the cystic plate is a visually identical task necessary in both “Dissection of Calot’s Triangle” and “Removal of Gallbladder from Liver Bed” phases. The correct phase is identified from prior knowledge that the cystic structures have already been clipped and divided).
3. Some of the temporal evidence collection occurs over a long period of time (consider priors about the length of each phase).

While extracting a perfect sufficient statistic of the past is hard due to estimator dimensionality and numerical training, the above two phenomena make

Algorithm 1: Forward estimate of surgery phase y_{t+1} .

input : Past LSTM hidden states $L_0 \cdot L_t$, past sufficient statistic s_0, \dots, s_t , next frame I_{t+1}

output: next frame hidden state L_{t+1} , next frame sufficient statistic s_{t+1} , next frame phase estimate.

- 1 Compute visual model output $f_V(I_{t+1})$;
- 2 Compute LSTM updated state L_{t+1} given $f_V(I_{t+1}), s_t, L_t$;
- 3 Compute current phase estimate y_{t+1} from L_{t+1} ;
- 4 Compute frame statistics $s_F(L_{t+1})$;
- 5 Compute new sufficient statistics s_{t+1} given past latent frame statistics and past sufficient statistics.

it possible to define a family of approximate sufficient statistics that can be computed from the data based on temporal aggregation of some transformation of the LSTM hidden state L_t . This makes it easier for the network to do both short-range temporal reasoning (such as change detection and visual processing), as well as medium- and long-range reasoning (such as counting past frames of each phase). The overall approach is presented in Algorithm 1 and illustrated in Figure 1.

Our architecture takes the past hidden LSTM layer, and passes it through a transform (the phase recognition module), to get a vector m_t , conceptualized as a temporal vector signal $\mathbf{M}_t = \{m_1 \dots m_t\}$. It then computes aggregate statistics of the transformed signal, resulting in a sufficient statistics feature stream $\mathbf{S} = \{s_1 \dots s_t\}$. By concatenating \mathbf{v}_t , it then feeds them to the current time phase LSTM inference as an augmented feature \mathbf{c}_t . After concatenation, an LSTM is applied taking \mathbf{c}_t as input to output the likelihood for each phase. Note that for both training and testing, the history memory \mathbf{M}_t is initialized with a Classic-LSTM model pretrained on training data, where the pretrained network structure is a variant of the proposed model by removing the SSM part. After the first iteration, the new LSTM prediction updates the history memory.

We note that several existing models fall within the family of functions described by this model, including temporal causal convolution (TCN) networks, PKI[7], and LSTMs. Furthermore, several novel sufficient statistic features are detailed in Section 2.2. The LSTM output space captures an approximate sufficient statistic on the past. The SSM module extracts from past information a reduced set of approximate sufficient statistics to make inference in the current time-point more efficient. Tailoring the choice of sufficient statistics can make it much easier for the network to learn specific dependencies and cues. While we describe this family regardless of resource constraints, in practice, many of the SSM features can be calculated in either $O(1)$ for computing-only or $O(1)$ for both computing and memory, as we will demonstrate.

2.2 Sufficient Statistic Features

Different choices of summarization S can make it easy for the network to learn long-term interactions. A few of the approaches explored in our experiments are described below.

Hidden Markov Model (HMM): HMM is a well-known statistical method for temporal filtering of discrete states. It is thus natural and intuitive to use HMM as a feature to encode temporal information. There are two main advantages of using HMM as a feature: 1) it provides smoother inference results, which provides an additional timescale of reasoning; 2) it can filter out impossible phase transitions using a state transition matrix, discouraging illogical phase transition inferences.

Cumulative Sum Likelihood (CSL): Temporal information can also be propagated by accumulating the LSTM inference likelihood in time.

$$\mathbf{f}_t = \log\left(\sum_{t'=1}^t (\mathcal{I}_l(\mathbf{m}_{t'})) + 1\right) \quad (1)$$

where \mathbf{f}_t represents the CSL at time step t , and \mathcal{I}_l represents thresholding of the elements of \mathbf{m} with a set of threshold levels l , with respect to the maximum probability phase at time t . The CSL feature enhances the network’s understanding of some global contexts and allows the network to capture both maximum-probability and probable interpretation of the phase at time t . It should have the capability to answer the question “where we are” in a surgery, including if certain phases have or have not already occurred. e.g. CSL can indicate that the phase “Divide Cystic Duct” has already been achieved; since it is a non-repeated event, we know that future frames cannot be classified as such.

Wavelets Transform: To capture temporal events at various time scales, we used a wavelet transform to summarize temporal information. We chose Gabor filter as a standard wavelet decomposition[13] and collect a filter bank with Gabor filters of different Gaussian envelope sizes to directly apply to the likelihood space along the time axis. The filtered results are then concatenated to gather the temporal information of different time scales. While this representation is $O(T)$ compute as described, there are efficient approximations for both Gabor and other wavelets. For example, Haar wavelets are trivial to compute at $O(1)$ complexity using integral images [4,11].

Causal vs. acausal features As the information can be propagated through time both in forward and backward directions, each of the features above can be built either in a causal manner or acausal manner, leveraging information from the future signal. We show the acausal SSM features as a proof of concept for offline analysis purposes [17]. For certain phases (e.g. checkpoint 1 in LC100 dataset), the inference of such phases may benefit from the future information.

3 Experiments

Datasets We evaluated our proposed method on two datasets:

1. **Cholec80** dataset contains 80 cholecystectomy videos each with 25 frames per second (fps). It provides annotations of tool presence and surgical phases (Table 1). The dataset is divided into a 40-40 split for training and testing.

| Index | Phase Name |
|-------|---------------------------|
| 0 | Preparation |
| 1 | Calot Triangle Dissection |
| 2 | Clipping and Cutting |
| 3 | Gallbladder Dissection |
| 4 | Gallbladder Packaging |
| 5 | Cleaning and Coagulation |
| 6 | Gallbladder Retraction |

Table 1. Phases in Cholec80

| Index | Phase Name |
|-------|--------------------------------|
| 0 | Port placement |
| 1 | Fundus retraction |
| 2 | Release GB peritoneum |
| 3 | Dissection of Calot’s triangle |
| 4 | Checkpoint 1 |
| 5 | Clip Cystic Artery |
| 6 | Divide Cystic Artery |
| 7 | Clip Cystic Duct |
| 8 | Divide Cystic Duct |
| 9 | Checkpoint 2 |
| 10 | Remove GB from liver bed |
| 11 | Bagging |
| 12 | Other step |

Table 2. Phases in MGH100

2. **MGH100** dataset contains 100 cholecystectomy videos each with 30 fps. It provides annotations of surgical phases (Table 2). The phases in MGH100 are more granular and clinically meaningful compared to Cholec80 (e.g., separating the broad category of “clipping and cutting” into separate tasks of clipping/cutting specific structures). We also added Checkpoints 1 and 2 to capture the decision points prior to clipping and removal of gallbladder, respectively. 80 videos are used for training while 20 are used for testing. For full details of the phases, see the supplementary material.

Prior work in surgical phase recognition has largely utilized public datasets such as Cholec80, which is annotated into long, visually distinct linear phases. In clinical practice, phases are often visually indistinct, of variable length, non-linear, repeating, and may be influenced by prior phases over the short and long-term – such characteristics are reflected in the annotation structure of phases in MGH100 (Table 2). These phases can be considered clinically actionable (i.e. phases at which influencing a surgeon’s actions could modify risk of complications) and align more closely with surgical decision-making [5].

Evaluation Metrics We evaluated our algorithms’ overall performance with the phased-averaged recall and precision, and F1-score across phases, in addition to total video accuracy (frames correctly inferred/total frames) [14].

Model Parameters We down-sampled all the videos to 1 fps. We kept parameters identical for the SSM-LSTM and Classic LSTM for a fair comparison. The LSTM hidden state was 64-dimensions. During training, batch size was set to 32. An adam [9] optimizer was applied with a learning rate of 0.0025. The number of training epochs was 20. We first trained the CNN model for 20 epochs then fine-tuned the CNN model during temporal model training. During Gabor feature calculation, 10 different Gaussian kernel sizes, σ , ranging from 10 to 30, were applied. After that, features of different sizes were concatenated together.

Training Strategy To facilitate memory efficiency during training, we detached the computation of the sufficient statistics from its effect on recent past

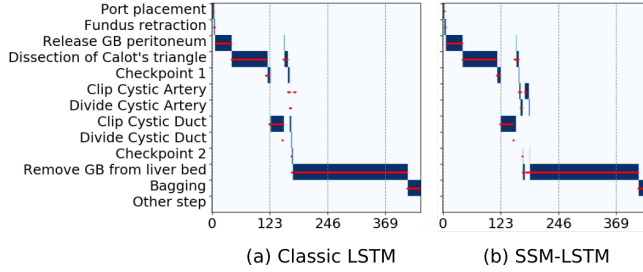


Fig. 2. Example result in MGH100 dataset (video 6). The x-axis is the time in seconds (s); y-axis rows represent a phase. The red line indicates the Ground truth trajectories. The color of the blue bar indicates the certainty of the algorithm, with darkness proportional to certainty.

analysis via the LSTM, which was trained with temporal sequences of length 8. We prevented oscillation of this numerical scheme using a lagged-step iteration, encouraging outputs that are close to the previous epoch. This has been shown in [2] to stabilize convergence, and under convexity assumptions of the cost function, can improve convergence properties.

Results The experiment results are shown both quantitatively and qualitatively. The results for Cholec80 dataset are in Table 3, benchmarking the SSM-LSTM model against several state-of-the-art models. Despite only leveraging phase labels without incorporation of other features (tool, kinematics) like *EndoNet* [17] or *MTRCNet-CL* [8], our proposed SSM-LSTM model has the best accuracy of 90.0% among the different models, with similar performance across precision, recall and F1 score. The result of our proposed method is then followed by an HMM for further smoothing. The results of combining causal and acausal features are shown as a proof of concept for offline applications. The results of

| | Model | Tool detection | Accuracy | Precision | Recall | F1 Score |
|---------|--------------------------------------|----------------|----------|-----------|--------|----------|
| Online | Binary Tool[8] | • | 47.5 | 54.4 | 60.2 | 57.2 |
| | EndoNet[17] | • | 81.7 | 73.7 | 79.6 | 76.5 |
| | SV-RCNet[7] | - | 85.3 | 80.7 | 83.5 | 82.1 |
| | MTRCNet-CL[8] | • | 89.2 | 86.9 | 88.0 | 87.4 |
| | SSM-LSTM (Proposed) | - | 90.0 | 87.0 | 83.0 | 84.9 |
| Offline | Causal + Acausal SSM-LSTM (Proposed) | - | 90.8 | 85.3 | 82.7 | 84.0 |

Table 3. Models' performance on the Cholec80 dataset. • indicates the methods are jointly trained to perform tool detection task. Our method outperforms all phase-only approaches (-) and reaches a slightly better accuracy than tool-based approaches, even though we do not use tool labels in training.

MGH100 datasets are in Table 4. The model's accuracy and F1 score benefited from each added feature. Take Fig 2, where applying SSM features helped the model accurately detect even the short phases “Clip Cystic Artery” and “Divide Cystic Artery.” With more clinically meaningful phase labels, the ground truth labels included alternating patterns (e.g. Fig 2), which differ from traditional linear workflows [17,20,10,6,22]. We noticed a substantial performance drop in

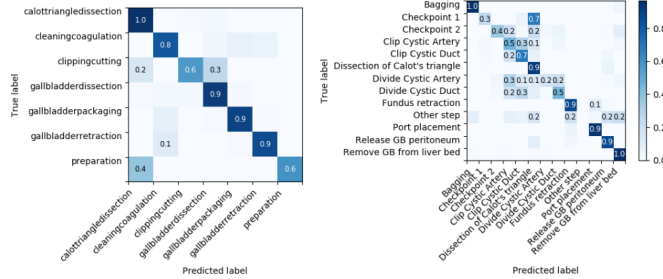


Fig. 3. Confusion matrix on Cholec80 dataset (left), MGH100 dataset (right)

traditional techniques that our SSM features helped ameliorate (cf. F1 scores in Table 4. The tradeoff between oversmoothing and evidence collection over multiple frames is fundamental in temporal process analysis. Our approach was able to improve significantly for short phases in this more challenging dataset.

We also analyzed SSM-LSTM performance on the individual phases, shown in Fig. 3. On the MGH100 dataset, the algorithm had good performance on long phases such as Release GB peritoneum, Dissection of Calots triangle, with accuracy over 90%. Short phase performance is not as good, for short phases are likely harder to infer due to harder to infer due to the lack of data variability (e.g. 37% of accuracy for phase checkpoint 2). However, with SSM, short phase performance has already improved compared with Classic LSTM, shown in Table 4, since the SSM provides additional information on the workflow structure.

We evaluated the accuracy of phase transitions and phase midpoints as per-segment statistics. For transition accuracy, a transition estimated within 10s of ground truth was considered correct. The SSM-LSTM achieved transition accuracy of 48.1% vs. Classic-LSTM at 39.0% for all phases. The accuracy for phase midpoint was 63.69% for SSM-LSTM vs. 56.23% for Classic LSTM. The performance benefits from the SSM module for both phase and transition inference, likely due to a better inference of phase start/end points and phase duration.

| Models | Accuracy | Precision | Recall | F1 Score | 1-3s | 4-10s | 11-30s | 31-60s | >60s | |
|--------|---------------------|-----------|--------|----------|------|-------|--------|--------|------|------|
| Online | LSTM | 83.3 | 50.2 | 51.6 | 50.9 | 12.5 | 40.6 | 47.0 | 63.1 | 91.7 |
| | Gabor | 84.1 | 51.2 | 57.4 | 54.1 | 15.6 | 44.1 | 53.4 | 66.4 | 90.2 |
| | CSL | 85.4 | 58.8 | 60.0 | 59.4 | 20.3 | 45.6 | 54.7 | 63.5 | 93.0 |
| | SSM | 85.6 | 59.4 | 61.5 | 60.4 | 31.2 | 51.6 | 58.2 | 64.4 | 93.0 |
| | Offline Acausal SSM | 86.8 | 61.9 | 65.4 | 63.6 | 35.9 | 52.4 | 64.3 | 64.7 | 93.0 |

Table 4. Models' performance on the MGH100 dataset. In the left part The results text relates the dataset characteristics to the F1-accuracy differences. The right part is the accuracy for phases of different durations. Our algorithm significantly improves short and challenging phase segments.

4 Conclusions

Overall, in this paper we propose a novel SSM-LSTM model that aggregates temporal information to assist LSTM inference. The proposed model has been validated on two large surgery datasets, Cholec80 and MGH100, achieving state-of-the-art performance. The proposed method contributes a key dependency for understanding long-range, clinically relevant temporal interactions in surgical workflows.

References

1. Aksamentov, I., Twinanda, A.P., Mutter, D., Marescaux, J., Padov, N.: Deep neural networks predict remaining surgery duration from cholecystectomy videos. In: International Conference on Medical Image Computing and Computer-Assisted Intervention. pp. 586–593. Springer (2017)
2. Attouch, H., Bolte, J., Redont, P., Soubeyran, A.: Proximal alternating minimization and projection methods for nonconvex problems: An approach based on the kurdyka-łojasiewicz inequality. *Mathematics of Operations Research* **35**(2), 438–457 (2010)
3. Bengio, Y., Simard, P., Frasconi, P.: Learning long-term dependencies with gradient descent is difficult. *IEEE transactions on neural networks* **5**(2), 157–166 (1994)
4. Crow, F.C.: Summed-area tables for texture mapping. In: Proceedings of the 11th annual conference on Computer graphics and interactive techniques. pp. 207–212 (1984)
5. Hashimoto, D.A., Axelsson, C.G., Jones, C.B., Phitayakorn, R., Petrusa, E., McKinley, S.K., Gee, D., Pugh, C.: Surgical procedural map scoring for decision-making in laparoscopic cholecystectomy. *The American Journal of Surgery* **217**(2), 356–361 (2019)
6. Hashimoto, D.A., Rosman, G., Witkowski, E.R., Stafford, C., Navarette-Welton, A.J., Rattner, D.W., Lillemoe, K.D., Rus, D.L., Meireles, O.R.: Computer vision analysis of intraoperative video: automated recognition of operative steps in laparoscopic sleeve gastrectomy. *Annals of surgery* **270**(3), 414–421 (2019)
7. Jin, Y., Dou, Q., Chen, H., Yu, L., Qin, J., Fu, C.W., Heng, P.A.: SV-RCNet: workflow recognition from surgical videos using recurrent convolutional network. *IEEE transactions on medical imaging* **37**(5), 1114–1126 (2017)
8. Jin, Y., Li, H., Dou, Q., Chen, H., Qin, J., Fu, C.W., Heng, P.A.: Multi-task recurrent convolutional network with correlation loss for surgical video analysis. *Medical image analysis* **59**, 101572 (2020)
9. Kingma, D.P., Ba, J.: Adam: A method for stochastic optimization. preprint arXiv:1412.6980 (2014)
10. Kitaguchi, D., Takeshita, N., Matsuzaki, H., Takano, H., Owada, Y., Enomoto, T., Oda, T., Miura, H., Yamanashi, T., Watanabe, M., Sato, D., Sugomori, Y., Hara, S., Ito, M.: Real-time automatic surgical phase recognition in laparoscopic sigmoidectomy using the convolutional neural network-based deep learning approach. *Surgical Endoscopy* (Dec 2019)
11. Lewis, J.: Fast template matching. In: Vision Interface. pp. 120–123 (1995)
12. Litjens, G., Kooi, T., Bejnordi, B.E., Setio, A.A.A., Ciompi, F., Ghafoorian, M., Van Der Laak, J.A., Van Ginneken, B., Sánchez, C.I.: A survey on deep learning in medical image analysis. *Medical image analysis* **42**, 60–88 (2017)
13. Mallat, S.: A wavelet tour of signal processing. Elsevier (1999)
14. Padov, N., Blum, T., Ahmadi, S.A., Feussner, H., Berger, M.O., Navab, N.: Statistical modeling and recognition of surgical workflow. *Medical image analysis* **16**(3), 632–641 (2012)
15. Pascanu, R., Mikolov, T., Bengio, Y.: On the difficulty of training recurrent neural networks. In: International conference on machine learning. pp. 1310–1318 (2013)
16. Qin, Y., Pedram, S.A., Feyzabadi, S., Allan, M., McLeod, A.J., Burdick, J.W., Azizian, M.: Temporal segmentation of surgical sub-tasks through deep learning with multiple data sources. arXiv preprint arXiv:2002.02921 (2020)

17. Twinanda, A.P., Shehata, S., Mutter, D., Marescaux, J., De Mathelin, M., Padoy, N.: Endonet: A deep architecture for recognition tasks on laparoscopic videos. *IEEE transactions on medical imaging* **36**(1), 86–97 (2016)
18. Twinanda, A.P., Yengeri, G., Mutter, D., Marescaux, J., Padoy, N.: Rsdnet: Learning to predict remaining surgery duration from laparoscopic videos without manual annotations. *IEEE transactions on medical imaging* **38**(4), 1069–1078 (2018)
19. Vaswani, A., Shazeer, N., Parmar, N., Uszkoreit, J., Jones, L., Gomez, A.N., Kaiser, L., Polosukhin, I.: Attention is all you need. In: *Advances in neural information processing systems*. pp. 5998–6008 (2017)
20. Volkov, M., Hashimoto, D.A., Rosman, G., Meireles, O.R., Rus, D.: Machine learning and coresets for automated real-time video segmentation of laparoscopic and robot-assisted surgery. In: *2017 IEEE International Conference on Robotics and Automation (ICRA)*. pp. 754–759. IEEE (2017)
21. Yu, F., Koltun, V.: Multi-scale context aggregation by dilated convolutions. In: Bengio, Y., LeCun, Y. (eds.) *4th International Conference on Learning Representations, ICLR 2016, San Juan, Puerto Rico, May 2-4, 2016, Conference Track Proceedings* (2016), <http://arxiv.org/abs/1511.07122>
22. Zisimopoulos, O., Flouty, E., Luengo, I., Giataganas, P., Nehme, J., Chow, A., Stoyanov, D.: DeepPhase: Surgical Phase Recognition in CATARACTS Videos. *arXiv:1807.10565 [cs, stat]* (Jul 2018)